QUASI STATIC ANKLE/FOOT COMPLEX BEHAVIOR: EXPERIMENTAL TESTS AND NUMERICAL SIMULATIONS

Catherine MASSON - Dominique CESARI - Frédéric BASILE
I.N.R.E.T.S., FRANCE
Muriel BEAUGONIN - Alain TRAMECON - Jean-Christophe ALLAIN - Eberhard HAUG
ESI GROUP, FRANCE

ABSTRACT

Quasi static axial loads were applied to cadaveric foot/ankle complexes in order to quantify the mechanical response of the biological tissues. The load-displacement characteristics of the foot were established and the associated injuries were noticed. The results showed comparable responses for the 2 feet of the same subject, but different responses from one subject to another. Injuries were essentially distensions of muscle in the mid plane of the plantar section. These results were used for the validation of a finite element numerical model of the ankle-foot complex. This model includes deformable parts and the representation of the cortical and trabecular bones. Some of the soft tissues have been added. Static foot compression simulations have been performed. This study showed that the global kinematics of the foot is well represented. The influence of the cortical bone resistance has been shown. Two kinds of compression collapse have been found depending on the yield stress value of the cortical bone, using a constant value of the trabecular bone yield stress.

ROAD ACCIDENTS is the leading cause of mortality for those under 40 years old in the industrialised countries (Bedewi, 1995). A considerable attention was thus turned to the protection of the lethal functions of car occupants, namely of the head and the torso, with the application of the belt and more recently of the airbag. This improvement underlined the relative weak protection brought to the lower limbs. However the foot-ankle complex injuries could require a treatment and a long-term rehabilitation and indeed could lead to a permanent impairment. A fracture of the calcaneum, for example, could induce to damages with an moderate long term impairment: walking limited, need of orthopaedic device to control pain (MAN, 1997). But if the type of the

injuries of the foot-ankle complex, in a frontal collision, would be predictable, mechanisms that cause them are not clearly established.

The aim of this work was to improve and to add biomechanical understanding of the response of the foot-ankle complex to static stress. At first, tests on biological material were carried out at the INRETS Laboratory of Applied Biomechanics to quantify the mechanical response of biological tissues. The reaction forces were measured in three support points of the foot subjected to a static axial compression. Then, a numerical simulation was made by ESI to understand the injury mechanisms found during these experimental tests. The PSI ankle/foot model was improved to simulate cortical bone fracture. Several parametric studies were performed that permit to define the influence of the strength of the cortical and of the trabecular bones. The simulations were performed with PAM-SAFE code.

TEST MATERIAL AND METHOD

SAMPLING AND INSTALLATION OF THE FOOT-ANKLE COMPLEX - A total of 5 human lower limbs were tested. They were amputated on 3 Post Mortem Human Subjects (2 males and 1 female) below the knee and preserved at 3°C in Winckler's preparation. Data on sex, age, weight, height of the donors are shown in Table 1.

Table 1 - Cadaver Physical Data

Subject Reference	Sex	Age	Weight (kg)	Height (mm)
85D (right foot)	M	83	69	1780
85G (left foot)	M	83	69	1780
86D (right foot)	F	88	53	1610
86G (left foot)	F	88	53	1610
88D (right foot)	M	80	57	1680
Mean		84	60	1692
Standard deviation		3,5	8	85

Prior to testing, the osseous integrity of the test samples was verified by X-Ray radiographs taken in 2 planes, the sagittal plane and the frontal plane. The proximal ends of the tibia and the fibula were denuded of their muscular insertions on fifteen centimeters below the cutting section and held captive in a square tube with cement. Particular attention was paid to keep the tibial axis vertical. The three support points of the foot, the calcaneum (C), the head of the 1st metatarsus (A), and the head of the 5th metatarsus (B) were marked by doctors in anatomy (Figure 1). The details of these bones are clearly distinguished by palpation. The weight of the foot and the distances between the three support points of the foot (Table 2) were noted.

EXPERIMENTAL SETUP - The testing apparatus shown in Figure 1 was used. The leg inserted in the tube was suspended from a frame. A manual press allowed to apply an ascending load under a support plate that came into

contact with the sole. A sensor placed on the top of the square tube measured the total load.

Table 2 - Sampling dimensions

Subject	AB (mm)	AC (mm)	BC (mm)	Foot Weight (kg)
85D	70	160	150	1.30
85G	65	155	155	1.21
86D	60	120	115	1.00
86G	60	130	120	1.00
88D	65	135	120	1.10
Mean	64±4	140±17	132±19	1.12±0.13

Three load sensors measured the response of the sole. They were fixed on the support plate, with a mobile fixation system in the horizontal plane that allows to place a sensor under each support point and to respect the different foot morphologies. The foot-ankle complex was loaded by steps of 200 N. Between each loading, the displacement was held constant during 2 minutes. The load then relaxed to a limit which is noted. A displacement sensor attached to the frame gave the linear displacement of the plate (Δz). The position and orientation of the foot were provided by two photographs, in a front and a side view. The test was stopped when the total load reached 4000 N or when the foot was obviously fractured.

INSTRUMENTATION - The sensors placed under the foot were standard Kistler 9021A load cells with a calibrated range of 35 kN, connected to quasi static charge amplifier with a large time constant (Kistler amplifiers). The measurement of the total load was done by a force bonded foil strain gauges sensor TME F 521 TC (measure range 25 kN) with a accuracy of 1 N. The displacement was measured with a laser cell Matsushita of extent 250 mm.

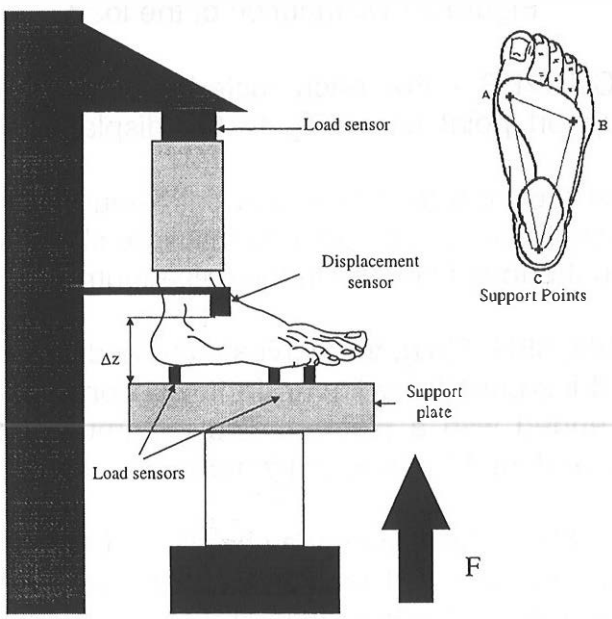

Figure 1 - Experimental device

RESULTS

DISTRIBUTION OF THE LOADS AT THE SUPPORT POINTS - The load distribution on the support points in comparison with the total load (Figure 2) indicated that between 60 and 80% of the total load was transmitted by the calcaneum, 7% by the first metatarsus and 11% by the fifth metatarsus. This distribution of pressure, and in particular the action of the calcaneum in the transmission, was comparable with the transmission of the body weight, in which the posterior tuberosity and the postero-external facet of the calcaneum carry 3/5 of the weight of the body (Bouchet).

In two cases (85D, 85G) the sum of the loads on the calcaneum, on the 1st metatarsus and on the 5th metatarsus was equal to the total load. In two cases, the sum of the responses of the three support points was inferior by 20%, and in one case, 86G, by 30%. This could be caused by a sliding friction in the test apparatus or a rotation of the foot inducing additional contact points.

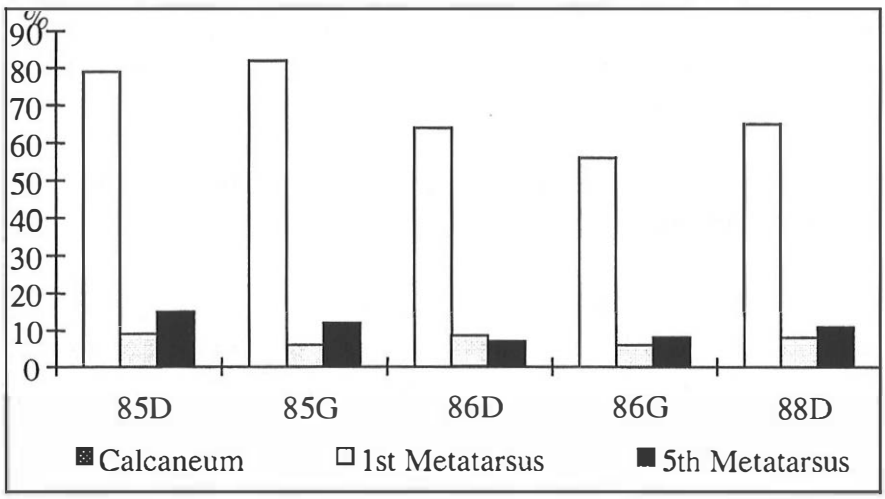

Figure 2 - Distribution of the load

LOAD STRAIN CURVES - For each tested foot, the total load and the reaction of each support point according to the displacement are presented (Figure 3).

For the five tested feet, the total load and calcaneum response curves are similar in shape. Discontinuities in the responses were clearly distinguished and were simultaneous in the total load and in the calcaneum response.

In three cases (85D, 85G, 88D), the curves may be divided into two parts. In the first part the load increase fairly linear. In the second part, the relationship was nonlinear and ended with a plateau. The maximum load was less than 2500 N and was reached for 11 mm displacement.

In two cases (86D, 86G), the curves may be divided into two parts. The load increased exponentially in the first part and linearly in the second part. The applied total load reached 3500 N before, in one case, a brutal decrease.

The shape of these curves seems to show that the elastic effects (linear phase) were predominant, due to elastic substructures of the foot-ankle complex. The slope of the linear phase of the total load curve may be taken as "elastic stiffness" and is listed Table 3.

Table 3 – Elastic stiffness

Subject	85D	85G	86D	86G	88D
Elastic stiffness (N/mm)	160	160	300	300	300

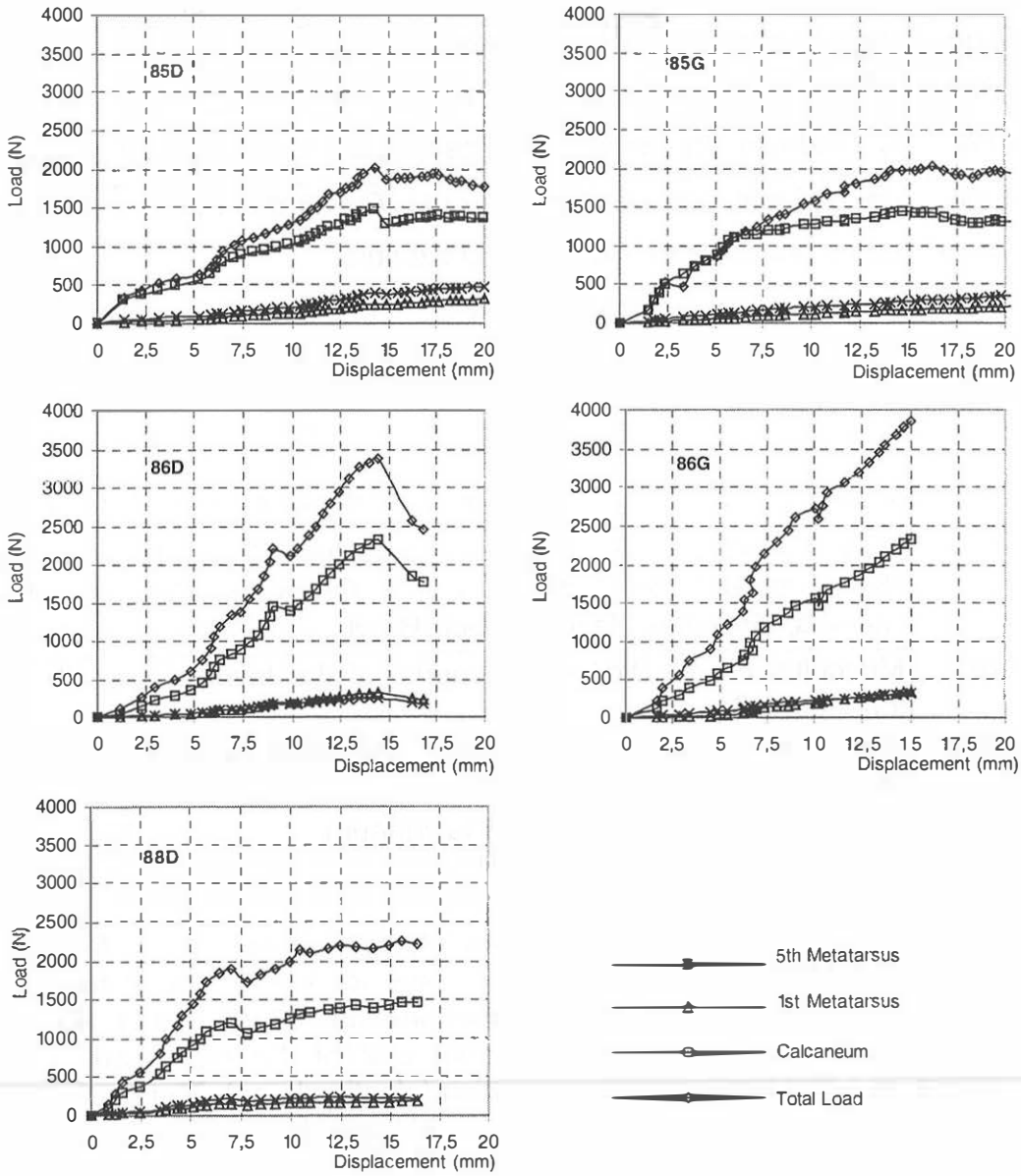

Figure 3 – Load-Displacement curves

NECROPSIC RESULTS - After testing, radiographs were taken and pre- and post-radiographs were analysed and compared. Each foot-ankle complex was then autopsied.

Table 4 lists the injuries: essentially straining of muscles, in the plantar section, in the intermediate and internal portions and in the mid plane. Very few fractures or osseous lesions were observed. Note that the foot was submitted to static load and that the threshold of the total load, fixed to 4000 N, was perhaps too low to cause osseous injuries. Time localization of the various types of injuries was not possible, although curves 86D and 88D (Figure 3) exhibited evidence of some local failure near 10 and 7.5mm of displacement, respectively.

Table 4 - Injuries

85D	*straining*	deep plantar aponevrosis, Musculus Quadratus Plantae
	*effraction**	talo-navicular and talo-cuboïdal capsules
	fracture	Cuboideum, 4th metatarsalia, settling-fracture of the calcaneum
85G	*straining*	deep plantar aponevrosis, Musculus Quadratus Plantae
	*effraction**	talo-navicular and talo-cuboïdal capsules
86D	*rupture*	Musculus Flexor Digitorum Brevis, at the level of the 2nd and 3rd toes
	straining	Musculus Flexor Hallucis Longus, Musculus Flexor Digitorum Longus, Musculus Abductor Hallucis
86G	*rupture*	Musculus Flexor Digitorum Brevis, at the level of the 2nd toe Musculus Flexor Digitorum Longus, at the level of the 4th toe
	straining	Musculus Quadratus Plantae, Musculus Flexor Hallucis Longus, Musculus Abductor Hallucis, Caput Obliquum Musculus Adductor Hallucis, Musculus Flexor Hallucis Brevis
88D	*rupture*	Musculus Flexor Digitorum Longus, at the level of the 4th and 5th toes (partial)
	straining	Musculus Flexor Digitorum Brevis, Musculus Flexor Hallucis Longus, Musculus Quadratus Plantae
	fracture	settling-fracture of the Tiberis Calcaneum

*anatomical terminology

CONCLUSION - The load-displacement characteristics of the foot-ankle complex have been established. The responses for the 2 feet of the same subject are comparable but results differ from one subject to another. However the general response of each support point and of the total load can be schematised by a first increasing linear portion (elastic phase). The slope of this linear phase is ranged from 160 N/mm to 300 N/mm (mean 224) for the total load, from 120 N/mm to 215 N/mm (mean 169) for the calcaneum response, from 19 N/mm to 38 N/mm (mean 28) for the 1st metatarsus response, and from 14 N/mm to 28 N/mm (mean 5) for the 5th metatarsus response. Then a plateau is noticed in 3 out of 5 cases.

If discontinuities in loading curves were clearly distinguished, they could not be directly attributed to specific injuries. Besides, the muscles (the more injured) are formed with many fibers and these fibers do not necessarily break together because of their different lengths and directions. The rupture of these tissues is therefore progressive. This explains that the number of observed load discontinuities is not equal to the number of detected injuries.

SIMULATION

ANKLE/FOOT MODEL DESCRIPTION –

Geometry -The finite element model corresponds to an "average" right foot (cf. Figure 4). The X-axis is horizontal and oriented in posterior-anterior direction, the Y-axis is horizontal in the external-internal direction and the Z-axis completes a right handed rectangular cartesian coordinate system.

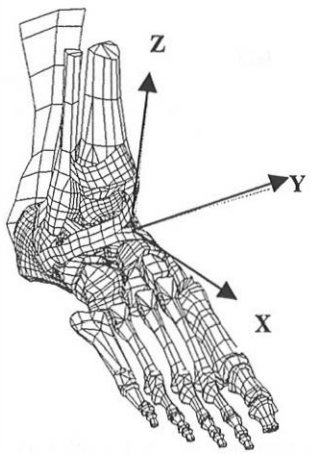

Figure 4: Ankle/Foot Model in Global Axis System

Bone modeling - In a previous paper (Beaugonin, 1997), the following bones were modelled as elastic deformable bodies: the fibula, tibia, talus, navicular bone and the cuboid. The cortical bone has been changed to elastic plastic thin shell elements with damage, while inelastic crushable foam solid elements are used for the trabecular bone. The rest of the foot bones were kept rigid. The damageable model contains a total of 5473 shells and 788 solid elements. The mesh for each damageable cortical bone is presented in Figure 5.

Equivalent soft tissue modeling - The padding effect provided by the layer of fatty tissue and skin of the sole was modeled using soft contact springs, the deformability of which takes into account the behavior of the padding.

Special care was given to the modeling of the following plantar soft tissue (Figure 6):
- Flexor digitorum brevis muscle and tendons,
- Plantar aponeurosis,
- Abductor hallucis.

Those components are seen to present particular damage in the PMHS tests. Therefore, they were added to the existing model in order to simulate their elongation, distension and breaking. Non linear elastic material properties found in the anatomical and biomechanical literature were taken (Yamada, 1970) (Annex Figures 13 (a) to (c)).

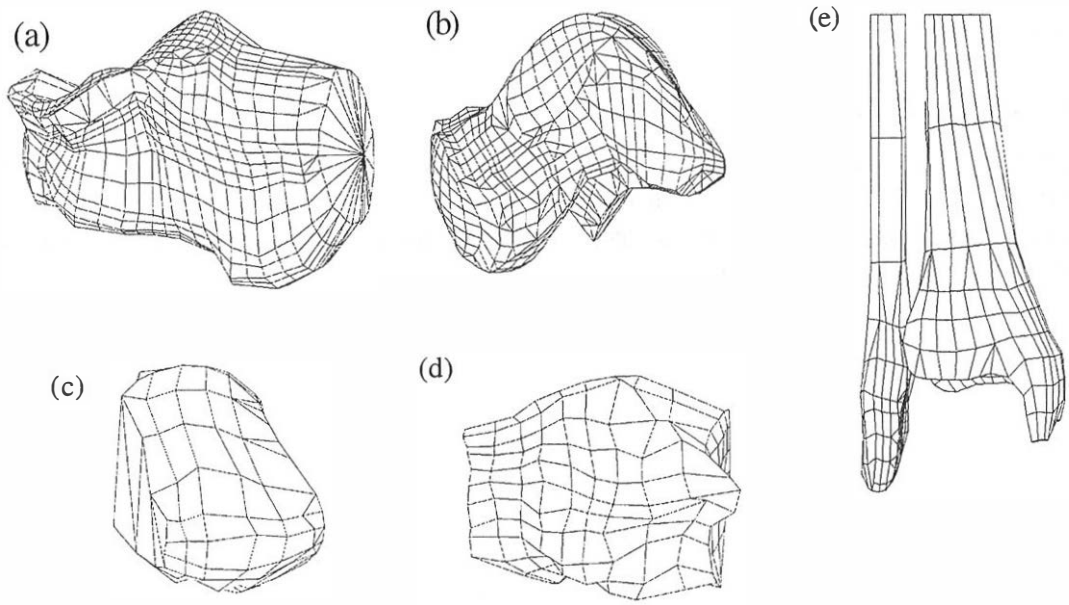

Figure 5: Cortical Bone Damageable Model of: (a) Calcaneum, (b) Talus, (c) Cuboid, (d) Navicular Bone, (e) Tibia and Fibula

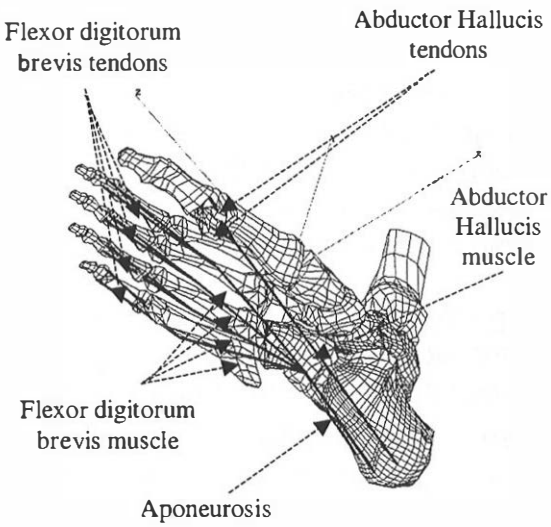

Figure 6: Added Plantar Soft Tissues

Material Properties - The soft tissues, ankle ligaments, retinacula and the Achilles tendon, have been modeled using linear and nonlinear elastic membranes. The foot ligaments are represented by bar elements with non linear elastic behavior (Annex Figure 14).

Table 5 summarises the basic biological component characteristics used as a basis of the static test simulation.

Table 5: Value ranges of bone and soft tissue properties

Materials	Poisson's ratio	Young's Modulus (MPa)	Mass Density (10^{-9} t/mm^3)
Rigid bone	rigid body	rigid body	2
Cortical bone (deformable)	0.29	18000	2
Trabecular bone (deformable)	~ 0	100	0.5
Foot Ligament (Begeman, 1995)		See Annex Figure 14	1
Ankle Ligament (Begeman, 1995)	0.22	88.2	1
Retinaculum Longitudinal Direction (Yamada, 1970)	0.22	123.8	1
Retinaculum Transversal direction (Yamada, 1970)	0.22	111.2	1
Achilles tendon (Yamada, 1970)	0.22	574.5	1
Added Plantar Soft Tissues		see Annex Figures 13 (a) to (c)	1

SIMULATION OF THE STATIC TEST - For this simulation, the foot model was placed on two "platforms" (Figure 7). The measured plate displacement for the subject 85 D (right foot) experimental test was prescribed in the numerical simulation.

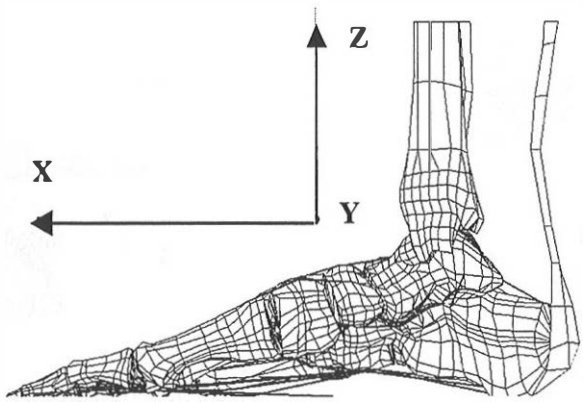

Figure 7: Simulation of Static Test

The preliminary results with elastic-plastic deformable bones were compared with the experiment. Table 6 presents the characteristics of the deformable bones.

Table 6: Deformable bone material parameters

Parameters	E (MPa)	ν	σ_v(MPa)	ε_p(initial damage) (%)
Cortical Bone (type 105)	18000	0.29	50	1
Trabecular Bone (type 1)	100	~ 0	12.5	1

SIMULATION RESULTS –

Global kinematics of the bones - During the vault collapse, the bone kinematics can be described in four main phases shown in Figure 8 (a) to (d).

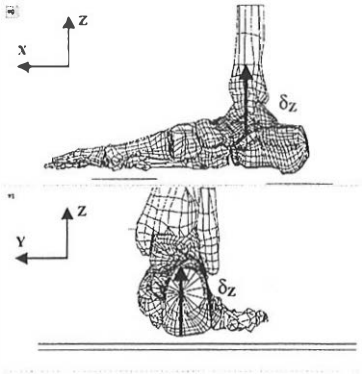

(a) All bones establish contact.
On the posterior side, the calcaneum contacts the talus, which contacts the tibia plafond.

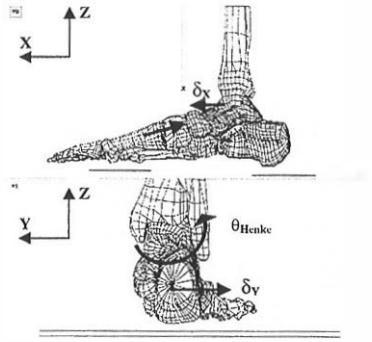

(b) A relative rotation between the talus and the calcaneum occurs about the axis of Henke, combined with a displacement of the talus along the Y-axis and the X-axis. Bones of the internal and external arches start to move towards each other, producing a force on the talus through the navicular bone and a force on the calcaneum through the cuboid

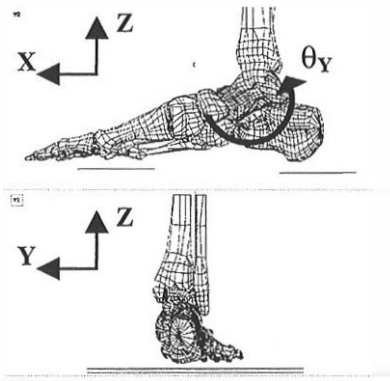

(c) A rotation between the talus and the tibia occurs about the Y-axis. The displacement of the talus along the X-axis is stopped by the navicular bone at a new equilibrium position of approximately δ_x=3mm from the initial state.

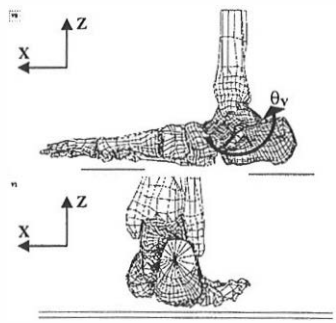

(d) The global Y-axis rotation of the talus and the calcaneum continues till the end of the simulation. An elongation of the plantar soft tissues and the foot ligaments of the internal arch occurs.

Figure 8: Ankle/foot bone kinematics

During this simulation, the calcaneum-cuboid joint opens, pointing at a local ligament or capsula injury, not found in the necropsies. Most of the foot ligaments are represented in the model but are modeled with one equivalent bar element because of their small dimensions. The musculoskeletal structure, in particular in the plantar region of the foot, is therefore represented only in an approximate fashion. The stiffness of the plantar ligaments was increased in order to control the local kinematics of the foot joints. The response curves of this simulation are presented in Figure 9.

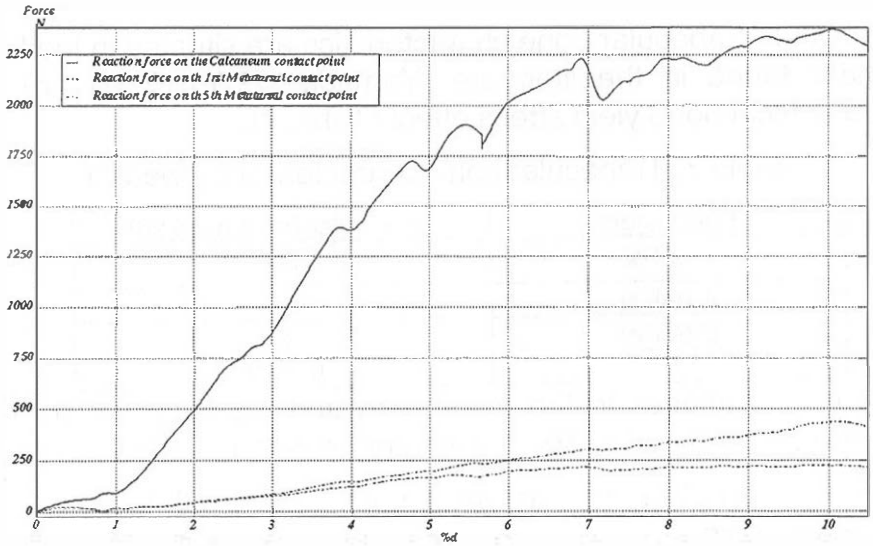

Figure 9: Reaction Force on Three Contact Points

The shapes of those curves are in good agreement with the average of the experiments (see Figure 3).

Influence of cortical bone characteristics with a weak trabecular bone – In view of the expected fluctuations between individuals, parametric studies have been conducted in order to check the influence of the yield stress σ_y in the cortical bone (from 50 MPa to 100 MPa). The properties of the trabecular bone were fixed at a low value for that purpose.

The cortical bone was modelled as an elastic-plastic material with isotropic damage (material type 105 in PAM-SAFE™).

In all following simulations, an inelastic crushable foam material has been used for the trabecular bone (material type 20 in PAM-SAFE™). The skeleton response of the foam follows an elastic-plastic law using a yield function. This response of the foam is considered directionally uncoupled (Poisson's ratio = 0). The characteristics of the material are described in Figure 10.

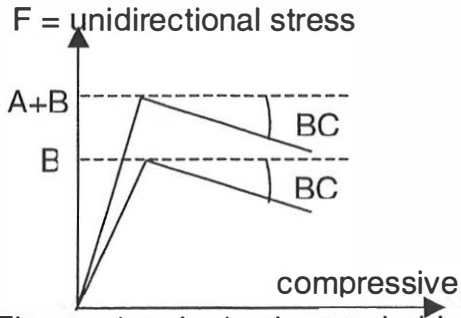

Tri-axial test: $F = A + B(1 + C\gamma)$

Hydrostatic test: $F = B(1 + C\gamma)$
where γ is the foam volume strain

Figure 10: Inelastic crushable foam material for the trabecular bones (material type 20 in PAM-SAFE™)

The chosen "weak" trabecular bone characteristics are situated in the lower part of the corridor found in the literature (Yamada, 1970). They are used to underline the cortical bone yield stress effect (Table 7).

Table 7: Trabecular bone characteristics ("weak")

Parameters	Trabecular Bone (type 20)
E (MPa)	100
A (MPa)	2.5
B (MPa)	3
C	0.0001

Distributions of damages in the calcaneum and the talus are presented in Figure11. Two competitive damage modes are obtained, namely

(a) Compression of the calcaneum (Figure 11 (a)) with low yield stress of the cortical bone

(b) Compression of the talus (Figure 11 (b)) with high yield stress of the cortical bone.

(a)

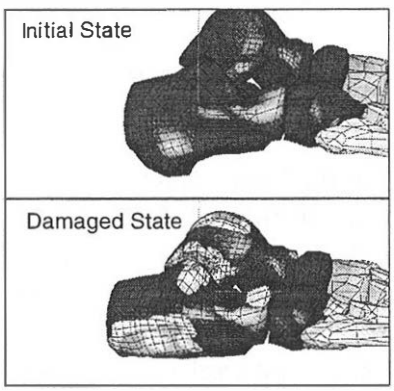

(b)

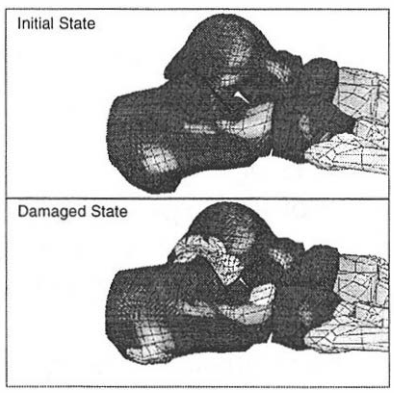

Figure 11: Damages in cortical bones: (a) σ_y = 50 MPa;(b) σ_y = 110 Mpa

(a) Low yield stress in the cortical bone (50 MPa): Damage appears in the calcaneum. The damaged areas start on the contact point with the load platform. The collapse of the vault increases, in particular near its internal side. Due to the resulting increased vault action, the navicular bone, top of the internal arch, compresses greatly the talus bone, restrained by the calcaneum. Its trabecular bone is crushed. Due to the breaking of the calcaneum, the talus is unloaded from below and fewer damages occur inside the talus (Figure 11 (a)).

(b) Yield stress in the cortical bone greater than 80 MPa: The von Mises stresses in the calcaneum remains now under the yield stress and massive damages are not present. Therefore the talus receives more loading from below. This loading of the talus induces damages on the interface between the calcaneum and the talus as shown in Figure 11 (b).

Influence of the trabecular bone - In all following simulations, the characteristics of cortical bone were set to the values shown in Table 8.

Table 8: Cortical bone material parameters (average)

Parameters	Cortical Bone (type 105)
E (MPa)	18000
ν	0.29
σ_y (MPa)	80
ε_0 (initial damage) (%)	1

A parametric study was performed concerning the influence of the trabecular bone yield stress. Four simulations with variations of the parameter B of the used material type 20 were made. The following values are used:

(a) B = 3 MPa, (b) B = 5 MPa,
(c) B = 7 MPa, (d) B = 10 MPa.

Damage distributions in each case are presented in Figure 12.

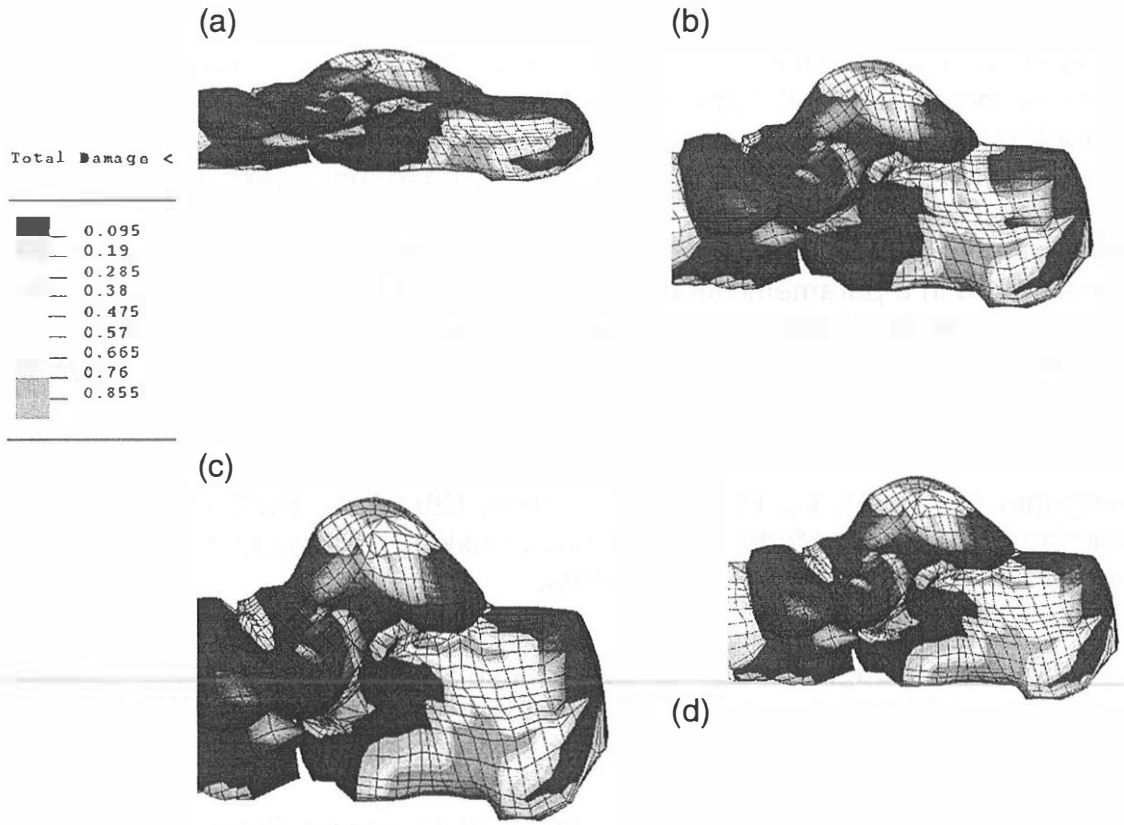

Figure 12: Damages in cortical bones with
(a) B = 3 MPa, (b) B = 5 MPa, (c) B = 7 MPa, (d) B = 10 MPa

These results show a great influence of the trabecular bone yield stress on the damage mode:

(1) If B is low (3 MPa and 5 MPa), the skeleton of the trabecular bone can collapse very easily. Therefore, when the cortical bone breaks, the trabecular bone collapses and a local compression occurs (cf. Figure 12 (a) and (b)): crush mode.

(2) If B is high (7 MPa and 10 MPa), the skeleton of material type 20 tends to stay elastic even after breaking of the cortical bone (cf. Figure 12 (c) and (d)). It does not collapse but provides resistance over the whole body of the bone. The result in the calcaneum is a shearing stress, which causes a fracture near the sustentaculum tali found during experimental tests: shear mode.

GENERAL CONCLUSION

The experimental study allowed to establish the load-strain characteristics and to list the injuries sustained by the foot-ankle complex submitted to a static compression. The response of each support point of the sole and of the total applied load can be schematised by a first increasing linear portion (elastic phase). If injuries have been noticed, it was not possible to determine the exact moments of their occurrences. The number of tested feet is too small to establish levels of tolerance or values of the critical threshold under this stress type. The tests provide nevertheless sufficient information for the validation of the numerical approach.

Based on the experiments carried out for this study, a crushable bone ankle/foot model (trabecular and cortical bone) has been developed. The model parameters for the bone fracture (trabecular and cortical bone) could not be calibrated completely on the reduced test data base, however. Therefore, and in view of the expected dispersion between individuals, the influence of the cortical and trabecular bone characteristics over the fracture mode has been demonstrated in a parametric study. Two competitive fracture modes were seen in the experiments. Additional tests may be required to ensure the validity of the simulation.

REFERENCES

Beaugonin M., Haug, E., ESI group, France; Césari D., INRETS, France; A Preliminary Numerical Model of the Human Ankle under Impact Loading. PLEI Conference,Washington, D.C., USA, 1995.

Beaugonin M., Haug, E., ESI group, France; Césari D., INRETS, France; Improvement of Numerical Ankle / Foot Model : Modeling of deformable Bone; Stapp Car Crash Conference, Alburquerque, New Mexico, USA, 1997.

Bedewi P.G., Bedewi N.E., 1996 Modeling of Occupant Biomechanics with Emphasis on the Analysis of Lower Extremity Injuries. http://gwuva.gwu.edu/ncac/ongoing/pubs/lower /lower.html

Begeman; P.; Direct Communication, Wayne State University, Detroit, Michigan, June 1995

Bouchet A., Cuilleret J., Anatomie topographique, descriptive et fonctionnelle. Le membre inférieur. Simep éditions

Manoli A., Prasad P., Levine R. Foot and Ankle Severity Scale. Foot & Ankle International. 1997 pp598-602

Yamada, H. – Editor Evans, F.G.; Strength of Biological Material. The William & Wilkins Company, Baltimore, 1970

ANNEX

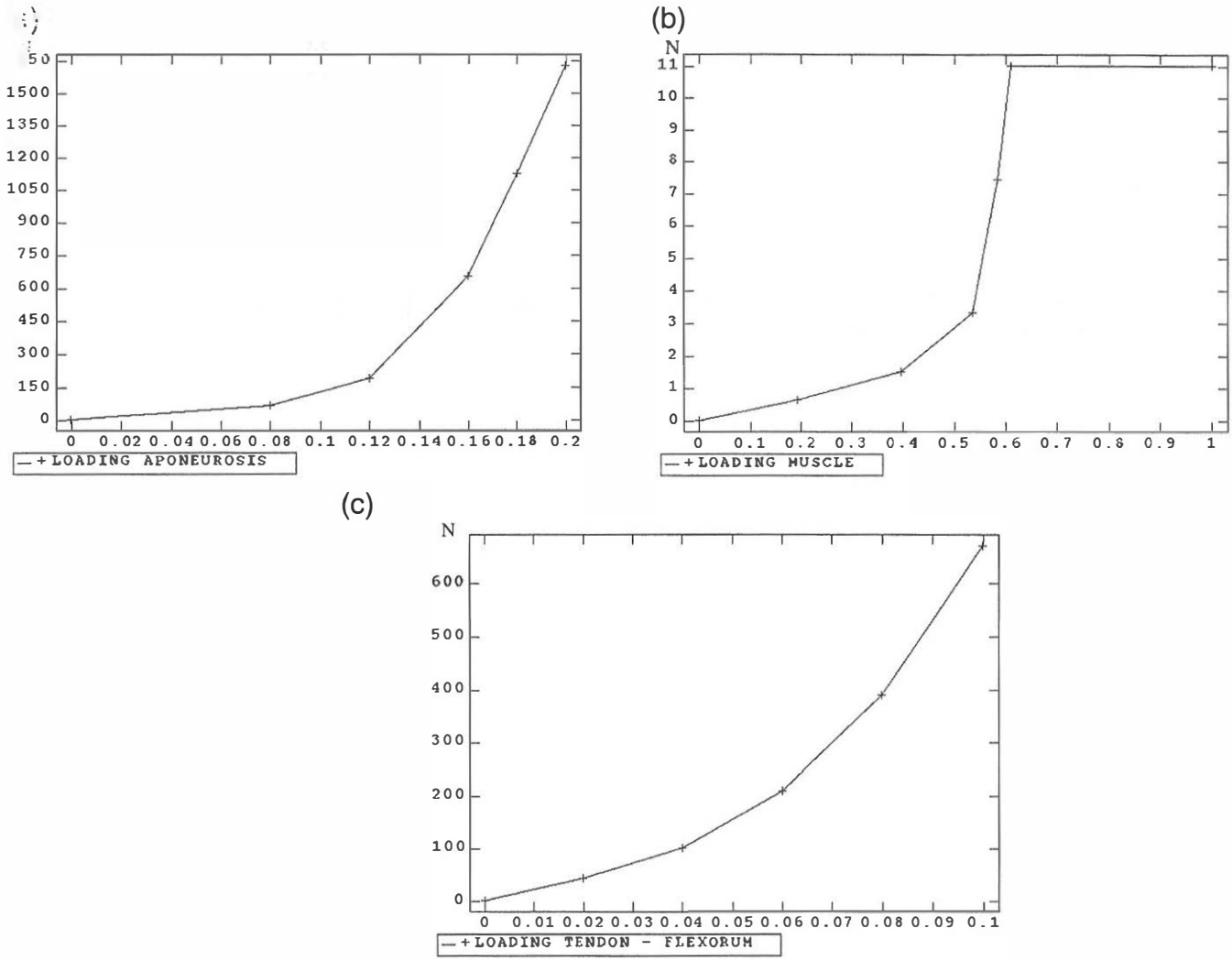

Figure 13: Force – strain curve of: (a) aponeurosis; (b) the plantar muscles; (c) the flexor tendons

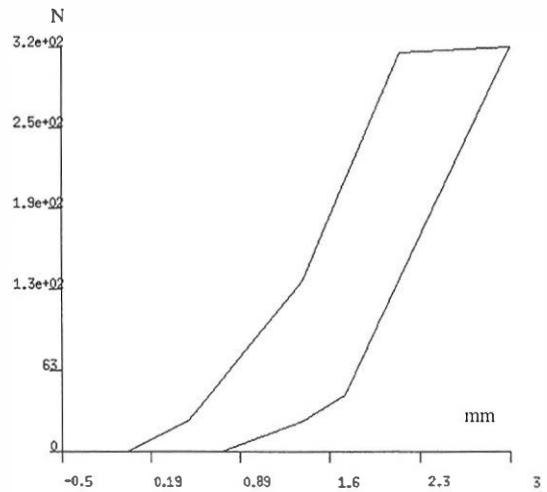

Figure 14: Force – elongation curve of foot ligaments